Self-modulation of nonlinear light in a vacuum enhanced by orbital angular momentum

Akitaka Watanabe
Solution Technology Department, Tokyo Gas Company, Ltd., 1-5-20 Kaigan, Minato-ku, Tokyo 105-8527, Japan

Kazunori Shibata *
Institute of Laser Engineering, Osaka University, 2-6 Yamada-Oka, Suita, Osaka 565-0871, Japan

(Received 20 July 2023; revised 1 March 2024; accepted 12 April 2024; published 3 June 2024)

Nonlinear optical effects in vacuum have been investigated as a means to verify quantum electrodynamics in a region of low photon energy. By considering nonlinear electromagnetic waves in a three-dimensional cylindrical cavity, we report that the orbital angular momentum of light strongly affects self-modulations in a long timescale. The variation in optical phase is shown to enhance the vacuum nonlinearity. Moreover, we demonstrate the time evolution of the phase shift and of the energy transfer between cavity modes, which may pave the way for verification experiments.

DOI: 10.1103/PhysRevA.109.063503

I. INTRODUCTION

Nonlinear electromagnetism in vacuum involves the interactions between electromagnetic fields. Such a nonlinearity is supposed to stem from virtual electron-positron pairs, i.e., the Heisenberg-Euler theory [1,2]. For the theory and other models [3,4], the lowest-order nonlinear electromagnetic Lagrangian density is characterized by two small parameters, $C_{2,0}$ and $C_{0,2}$. However, these values have not yet been identified experimentally.

The nonlinearity in vacuum is considered to cause peculiar phenomena such as magnetic monopoles [5]. Moreover, a correction brought by the nonlinearity is studied in astrophysics, e.g., on the radiation from pulsars or magnetars [6–8] and a state of black holes [5,9].

For the detection of vacuum nonlinearity, one proposal is to employ a high-intensity and ultrashort-pulse laser [10]. Another method is to utilize a mirror and a low- or modest-intensity laser, such as a waveguide [11], a ring laser [12], and cavity. Several experiments have been performed, e.g., the PVLAS (Polarizzazione del Vuoto con LASer) [13,14], BMV (Biréfringence Magnétique du Vide) [15], and OVAL (Observing VAcuum with Laser) [16] experiments, which aimed to detect vacuum birefringence.

A cavity system is capable of retaining light in a much longer time than short-pulse lasers. In a cavity, a resonant increase of nonlinear correction with time has been theoretically studied [17–20]. Recently, the appearance of large self-modulation in a long timescale has been reported in one- and two-dimensional cavities [21,22]. The self-modulation in the long timescale can become comparable to classical fields. For verification experiments, it is worthwhile to reveal characteristics of a large self-modulation in a long timescale in a three-dimensional cavity.

In this study, we consider a three-dimensional cylindrical cavity, with a modest-intensity laser and a static magnetic field. We elucidate that the orbital angular momentum of light completely changes the behavior of self-modulation. As an example of self-modulation, energy transfer among the cavity modes is demonstrated.

This manuscript is organized as follows. The basic notation, the considered system, and classical electromagnetic fields are explained in the next section. The resonant term in a linear approximation is given in Sec. III. In Sec. IV, the differential equations in Eq. (15) are derived. They are the key equations that describe the large self-modulation in a longer timescale. The solution of Eqs. (15) is given in Sec. V. Section VI is dedicated to demonstrating how the angular momentum of light changes the self-modulation. An experimental perspective is stated in Sec. VII. Final remarks are given in the last section.

II. NOTATION, SYSTEM, AND CLASSICAL TERM

We normalize electromagnetic fields by the electric constant ε_0 and the magnetic constant μ_0. The electric field $\boldsymbol{E}$ is multiplied by $\varepsilon_0^{1/2}$, and the magnetic flux density $\boldsymbol{B}$ is divided by $\mu_0^{1/2}$, respectively. Quantum electrodynamics predicts that the vacuum yields a nonlinear effect on electromagnetic fields via virtual electron-positron pairs [1,2,23]. By using two Lorentz invariants $F = \boldsymbol{E}^2 - \boldsymbol{B}^2$ and $G = \boldsymbol{E} \cdot \boldsymbol{B}$, the lowest-order nonlinear electromagnetic Lagrangian is given by

$$\mathscr{L} = \tfrac{1}{2}F + C_{2,0}F^2 + C_{0,2}G^2, \tag{1}$$

where $C_{2,0}$ and $C_{0,2}$ are the nonlinear parameters. The values in the Heisenberg-Euler theory are $C_{2,0} = \hbar e^4/(360\pi^2\varepsilon_0^2 m_e^4 c^7)$ and $C_{0,2} = 7C_{2,0}$, respectively [23–25], where $\hbar$ is Planck's constant divided by 2π, e is the elementary charge, m_e is the electron mass, and c is the speed of light.

*shibata-ka@ile.osaka-u.ac.jp

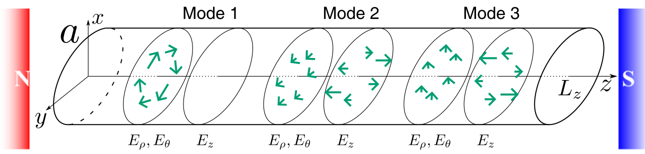

FIG. 1. The cylindrical cavity system with a perfect mirror. The electric fields for three eigenmodes are illustrated in the xy plane at $\rho = a/2$. The external magnetic flux density is symbolically shown by the N and S poles.

The electric flux density $\boldsymbol{D}$ and magnetic field $\boldsymbol{H}$ are derived by the partial derivatives of $\mathscr{L}$ with respect to $\boldsymbol{E}$ and $-\boldsymbol{B}$, respectively. The vacuum nonlinearity appears in these constitutive equations. The nonlinear Maxwell equations are

$$\begin{aligned} \nabla \times \boldsymbol{E} + \frac{1}{c}\frac{\partial \boldsymbol{B}}{\partial t} &= \boldsymbol{0}, \\ \nabla \cdot \boldsymbol{B} &= \boldsymbol{0}, \\ \nabla \times \boldsymbol{H} - \frac{1}{c}\frac{\partial \boldsymbol{D}}{\partial t} &= \boldsymbol{0}, \\ \nabla \cdot \boldsymbol{D} &= \boldsymbol{0}. \end{aligned} \tag{2}$$

A. System

The whole cylindrical cavity system is depicted in Fig. 1. The radius and height of the cylindrical cavity are given by a and L_z, respectively. The cavity mirror is supposed to be a perfect conductor. Then, the boundary conditions are determined. This system is dissipation-free, i.e., no energy loss from reflection.

B. Classical term

The total nonlinear electromagnetic field is divided into two parts. One is the well-known "classical term," which satisfies the linear classical Maxwell equations. As the classical term, we consider three eigencavity modes, i.e., standing waves. They have the same frequency ω. We call them modes 1, 2, and 3, respectively. The wave-number components in the radial and axial directions are given by $k_\rho = \lambda_{1j}/a$ and $k_z = n\pi/L_z$, where $n \in \mathbb{N}$ and λ_{1j} denotes the jth positive zero of the Bessel function J_1. The wave number is given by $k = (k_\rho^2 + k_z^2)^{1/2} = \omega/c$. We notate $T = \omega t$. In a cylindrical coordinate system (ρ, θ, z), the electric fields for each eigenmode $\boldsymbol{E}_{c1}$, $\boldsymbol{E}_{c2}$, and $\boldsymbol{E}_{c3}$ are given as

$$\begin{aligned} E_{c1\rho} &= 0, \\ E_{c1\theta} &= \frac{1}{\sqrt{2}} J_1(k_\rho \rho) \sin k_z z\,(f_c \cos T + f_s \sin T), \\ E_{c1z} &= 0, \end{aligned} \tag{3}$$

$$\begin{aligned} E_{c2\rho} &= -\frac{k_z}{2k}[J_0(k_\rho\rho) - J_2(k_\rho\rho)] \sin\theta \sin k_z z\,(g_c \cos T \\ &\quad + g_s \sin T), \\ E_{c2\theta} &= -\frac{k_z}{2k}[J_0(k_\rho\rho) + J_2(k_\rho\rho)] \cos\theta \sin k_z z\,(g_c \cos T \\ &\quad + g_s \sin T), \\ E_{c2z} &= \frac{k_\rho}{k} J_1(k_\rho\rho) \sin\theta \cos k_z z\,(g_c \cos T + g_s \sin T), \end{aligned} \tag{4}$$

$$\begin{aligned} E_{c3\rho} &= -\frac{k_z}{2k}[J_0(k_\rho\rho) - J_2(k_\rho\rho)] \cos\theta \sin k_z z\,(h_c \cos T \\ &\quad + h_s \sin T), \\ E_{c3\theta} &= \frac{k_z}{2k}[J_0(k_\rho\rho) + J_2(k_\rho\rho)] \sin\theta \sin k_z z\,(h_c \cos T \\ &\quad + h_s \sin T), \\ E_{c3z} &= \frac{k_\rho}{k} J_1(k_\rho\rho) \cos\theta \cos k_z z\,(h_c \cos T + h_s \sin T), \end{aligned} \tag{5}$$

where f_c, f_s, g_c, g_s, h_c, and h_s are amplitudes. These magnitudes are modest so as not to break the mirror. The corresponding magnetic flux densities $\boldsymbol{B}_{c1}$, $\boldsymbol{B}_{c2}$, and $\boldsymbol{B}_{c3}$ are determined uniquely. We also consider a constant static magnetic flux density $\boldsymbol{B}_s$ in the z direction, but not in the ρ or θ directions, because of the compatibility of Maxwell's equations and boundary conditions [26]. In summary, the classical electric field and magnetic flux density are given by $\boldsymbol{E}_c = \boldsymbol{E}_{c1} + \boldsymbol{E}_{c2} + \boldsymbol{E}_{c3}$ and $\boldsymbol{B}_c = \boldsymbol{B}_{c1} + \boldsymbol{B}_{c2} + \boldsymbol{B}_{c3} + \boldsymbol{B}_s$, respectively.

The classical electromagnetic energy in the cavity is given by

$$\begin{aligned} \int \frac{1}{2}(|\boldsymbol{E}_c|^2 + |\boldsymbol{B}_c|^2) dV = \frac{\pi a^2 L_z}{8}\big[\big(f_c^2 + f_s^2 + g_c^2 + g_s^2 \\ + h_c^2 + h_s^2\big) J_0(\lambda_{1j})^2 + 4B_s^2\big]. \end{aligned} \tag{6}$$

The classical orbital angular momentum is not zero only in the z component, i.e.,

$$\frac{1}{c}\int \rho(E_z B_\rho - E_\rho B_z) dV = -\frac{\pi a^2 L_z}{4\omega}(g_c h_s - g_s h_c) J_0(\lambda_{1j})^2. \tag{7}$$

We simply refer to the z component as "angular momentum."

In the following, we often use

$$\begin{aligned} X &= f_c^2 + f_s^2 + g_c^2 + g_s^2 + h_c^2 + h_s^2, \\ Y &= g_c h_s - g_s h_c, \end{aligned} \tag{8}$$

where $X > 0$ corresponds to the optical energy, and Y is the angular momentum. They do not express Cartesian coordinates. Note that $C_{2,0}X$ is dimensionless and practically $C_{2,0}X \ll 1$.

III. RESONANT INCREASE IN LINEAR APPROXIMATION

The classical term cannot satisfy Eq. (2). Let $\boldsymbol{E}_{\text{tot}}$ and $\boldsymbol{B}_{\text{tot}}$ be the total electromagnetic field, which satisfies Eq. (2). We call the difference $\boldsymbol{E}_{\text{tot}} - \boldsymbol{E}_c$ and $\boldsymbol{B}_{\text{tot}} - \boldsymbol{B}_c$ the "corrective term."

As long as the corrective term is much smaller than the classical term, a perturbative linear approximation can be applied. The polarization $\boldsymbol{P} = \boldsymbol{D} - \boldsymbol{E}$ and magnetization $\boldsymbol{M} = \boldsymbol{B} - \boldsymbol{H}$ of vacuum are approximated only by the classical term. They are notated as $\boldsymbol{P}_c$ and $\boldsymbol{M}_c$, respectively. We express the corresponding corrective term as $\boldsymbol{E}_n^{(0)}$ and $\boldsymbol{B}_n^{(0)}$. They satisfy the following equations:

$$\begin{aligned}
&\nabla \times \boldsymbol{E}_n^{(0)} + k\dot{\boldsymbol{B}}_n^{(0)} = \boldsymbol{0},\\
&\nabla \cdot \boldsymbol{B}_n^{(0)} = \boldsymbol{0},\\
&\nabla \times \boldsymbol{B}_n^{(0)} - k\dot{\boldsymbol{E}}_n^{(0)} = k\dot{\boldsymbol{P}}_c + \nabla \times \boldsymbol{M}_c,\\
&\nabla \cdot \boldsymbol{E}_n^{(0)} = -\nabla \cdot \boldsymbol{P}_c,
\end{aligned} \tag{9}$$

where an overdot expresses the differentiation with respect to T. The solution can be obtained by the method of separation of variables. The θ and z dependencies expanded in the Fourier series. The Fourier-Bessel expansion is employed for the ρ dependence. Then one obtains simple ordinal differential equations for T.

A part of the solution is a resonant term that increases with time, i.e., the secular term. For example, the E_θ component of the resonant term is given as

$$\begin{aligned}
E_\theta^{(\mathrm{reso})} = &\frac{1}{\sqrt{2}}(\tilde{D}_{1c}\cos T + \tilde{D}_{1s}\sin T)TJ_1(k_\rho\rho)\sin k_z z\\
&- \frac{k_z}{2k}(\tilde{D}_{2c}\cos T + \tilde{D}_{2s}\sin T)\\
&\times T[J_0(k_\rho\rho) + J_2(k_\rho\rho)]\cos\theta\sin k_z z\\
&+ \frac{k_z}{2k}(\tilde{D}_{3c}\cos T + \tilde{D}_{3s}\sin T)\\
&\times T[J_0(k_\rho\rho) + J_2(k_\rho\rho)]\sin\theta\sin k_z z.
\end{aligned} \tag{10}$$

It should be emphasized that the resonant term has the same spatial distribution as the classical mode. This feature is the same for the other components.

The coefficients $\tilde{D}_{1c},\ \tilde{D}_{1s},\ \tilde{D}_{2c},\ \tilde{D}_{2s},\ \tilde{D}_{3c}$, and $\tilde{D}_{3s}$ do not express the electric flux density and they are given as follows. Let $\Delta = k_\rho^2/k^2$ and

$$\begin{aligned}
S_1 &= \frac{1}{4\lambda_{1j}^2 J_0(\lambda_{1j})^2}C_{2,0}[8(1-\Delta+\Delta^2)I_+ + 7\Delta^2 I_-],\\
S_2 &= \frac{1}{48\lambda_{1j}^2 J_0(\lambda_{1j})^2}\{24C_{2,0}[-4\Delta(1-\Delta)I_+ + (4-4\Delta-\Delta^2)I_-] + C_{0,2}[8I_+ - (8-9\Delta^2)I_-]\},\\
S_3 &= \frac{1}{24\lambda_{1j}^2 J_0(\lambda_{1j})^2}\{8C_{2,0}[2(1+2\Delta-2\Delta^2)I_+ + (10-10\Delta+\Delta^2)I_-] - C_{0,2}[4I_+ - (4-3\Delta^2)I_-]\},\\
S_4 &= \frac{1}{24\lambda_{1j}^2 J_0(\lambda_{1j})^2}C_{2,0}[72(1-\Delta+\Delta^2)I_+ - 5(16-16\Delta+9\Delta^2)I_-],\\
S_5 &= \frac{1}{12\lambda_{1j}^2 J_0(\lambda_{1j})^2}\{C_{2,0}[-24(1-\Delta+\Delta^2)I_+ + (16-64\Delta+15\Delta^2)I_-] + 8C_{0,2}(1-\Delta)I_-\},
\end{aligned} \tag{11}$$

where

$$I_+ = \int_0^{\lambda_{1j}} xJ_1(x)^4 dx, \quad I_- = \int_0^{\lambda_{1j}} \frac{1}{x}J_1(x)^4 dx, \tag{12}$$

and let $\mathscr{A}_1 = f_c^2 + f_s^2$, $\mathscr{A}_{23} = g_c^2 + g_s^2 + h_c^2 + h_s^2$. The resonant coefficients are given by

$$\begin{aligned}
\tilde{D}_{1c} &= -\left(S_1\mathscr{A}_1 + S_2\mathscr{A}_{23} + 4\frac{k_\rho^2}{k^2}C_{2,0}B_s^2\right)f_s - S_3[(f_c g_c + f_s g_s)g_s + (f_c h_c + f_s h_s)h_s],\\
\tilde{D}_{1s} &= \left(S_1\mathscr{A}_1 + S_2\mathscr{A}_{23} + 4\frac{k_\rho^2}{k^2}C_{2,0}B_s^2\right)f_c + S_3[(f_c g_c + f_s g_s)g_c + (f_c h_c + f_s h_s)h_c],\\
\tilde{D}_{2c} &= -\left(S_2\mathscr{A}_1 + S_4\mathscr{A}_{23} + \frac{k_\rho^2}{k^2}C_{0,2}B_s^2\right)g_s - S_3(f_c g_c + f_s g_s)f_s + S_5 Y h_c,\\
\tilde{D}_{2s} &= \left(S_2\mathscr{A}_1 + S_4\mathscr{A}_{23} + \frac{k_\rho^2}{k^2}C_{0,2}B_s^2\right)g_c + S_3(f_c g_c + f_s g_s)f_c + S_5 Y h_s,\\
\tilde{D}_{3c} &= -\left(S_2\mathscr{A}_1 + S_4\mathscr{A}_{23} + \frac{k_\rho^2}{k^2}C_{0,2}B_s^2\right)h_s - S_3(f_c h_c + f_s h_s)f_s - S_5 Y g_c,\\
\tilde{D}_{3s} &= \left(S_2\mathscr{A}_1 + S_4\mathscr{A}_{23} + \frac{k_\rho^2}{k^2}C_{0,2}B_s^2\right)h_c + S_3(f_c h_c + f_s h_s)f_c - S_5 Y g_s.
\end{aligned} \tag{13}$$

An increase of high harmonics can occur only for particular cavity sizes of a/L_z [19]. We do not treat such a special situation here.

The corrective term within the linear approximation can be written in the form of "$\boldsymbol{E}_n^{(0)} = \boldsymbol{E}^{(\mathrm{reso})}$+nonresonant terms." The second term on the right-hand side is always much smaller than the classical term, about $C_{2,0}X$ times. In contrast, the resonant term increases with T. Consequently, the linear approximation is violated in a certain time.

IV. LEADING PART BEYOND THE LINEAR APPROXIMATION

As is explained in Eq. (10), the resonant term of $\boldsymbol{E}_n^{(0)}$ and $\boldsymbol{B}_n^{(0)}$ has the same spatial distribution with the classical term. Therefore, the total electromagnetic field can be given as "classical term+resonant term+other extremely small terms," as long as the linear approximation is valid. The first two terms can be interpreted as the amplitudes of the classical term are slightly modulated. This viewpoint leads us to the assumption that the total electromagnetic field can be expressed in the form

$$\text{modulated classical term} + \text{vanishingly small terms.} \tag{14}$$

Here, the word "modulated" means that the amplitudes slowly vary with time. The spatial distributions remain in the original classical term.

Consider the form at a specific time and calculate the corrective term afterward. As long as the linear approximation is applicable, the dominant part of $\boldsymbol{P}$ and $\boldsymbol{M}$ can be composed of the modulated classical term. As a result, the linearized corrective term can again be expressed by a sum of resonant and vanishingly small nonresonant terms. The resonant term has the same spatial distribution as the classical term. This fact supports the assumption.

Hereafter, we call the modulated classical term the "leading part." Furthermore, we refer to the term "long timescale" only to indicate that we are considering beyond the linear approximation.

Handling the leading part in the long timescale can be accomplished by regarding the amplitudes $f_c,\ f_s,\ g_c,\ g_s,\ h_c$, and h_s as "time-dependent." These are assumed to change slowly enough compared to $2\pi/\omega$ from a viewpoint of multiscale analysis.

By substituting Eq. (14) into the nonlinear Maxwell equations in Eq. (2) and discarding all the vanishingly small terms, nonlinear simultaneous differential equations for slowly varying amplitudes $f_c,\ f_s,\ g_c,\ g_s,\ h_c$, and h_s are derived as

$$\begin{aligned}
&\dot{f}_c = \tilde{D}_{1c}, \quad \dot{f}_s = \tilde{D}_{1s},\\
&\dot{g}_c = \tilde{D}_{2c}, \quad \dot{g}_s = \tilde{D}_{2s},\\
&\dot{h}_c = \tilde{D}_{3c}, \quad \dot{h}_s = \tilde{D}_{3s}.
\end{aligned} \tag{15}$$

The right-hand sides are given by Eq. (13). They are also time-dependent since the amplitudes are time-dependent. Note that Eqs. (15) conserve X and Y as constant. They correspond to the "classical" parts of the total energy and angular momentum. For this reason, we conclude that the assumption and Eqs. (15) are reasonable.

We solve the differential equations for the following initial values:

$$\begin{aligned}
&f_c(0) = 0, \quad f_s(0) = A_{(1)},\\
&g_c(0) = A_{(2)} \sin\varphi_{(2)}, \quad g_s(0) = A_{(2)} \cos\varphi_{(2)},\\
&h_c(0) = A_{(3)} \sin\varphi_{(3)}, \quad h_s(0) = A_{(3)} \cos\varphi_{(3)},
\end{aligned} \tag{16}$$

where $A_{(1)},\ A_{(2)}$, and $A_{(3)}$ are the classical amplitudes of modes 1, 2, and 3, and $\varphi_{(2)}$ and $\varphi_{(3)}$ are the relative phases of modes 2 and 3 to mode 1, respectively.

To solve Eqs. (15), we introduce an auxiliary function $\alpha = (f_c^2 + f_s^2)/X$. This expresses the energy ratio of mode 1. It is solved in the Appendix. In particular, we derive another conserved quantity Z.

V. SOLUTION OF EQS. (15)

The solution of Eqs. (15) can be written down by using the obtained α. Please refer to the Appendix for $Z,\ Q_1(\alpha),\ Q_2(\alpha),\ c_1,\ c_2,\ \mathscr{X},\ \tilde{\mathscr{X}},\ \mathscr{Y},\ \tilde{\mathscr{Y}},\ \xi,\ \mathfrak{q}_{1-},\ \mathfrak{q}_{2-},\ \tilde{\mathfrak{s}}$, and $Y_{\max}$.

First, we show f_c and f_s. If $\alpha = 0$ at a specific time, it is always zero. Consequently, $f_c = 0$ and $f_s = 0$. Otherwise, by using

$$\begin{aligned}
\Psi = {}& \frac{1}{2}(S_1 - S_4)X \int_0^T \alpha(\tau)d\tau + \left(S_4 X + \frac{k_\rho^2}{k^2} C_{0,2} B_s^2\right)T\\
&- \frac{Z}{2}\int_0^T \frac{1}{\alpha(\tau)}d\tau,
\end{aligned} \tag{17}$$

these are calculated as

$$f_c = -\sqrt{X\alpha}\sin\Psi, \quad f_s = \sqrt{X\alpha}\cos\Psi. \tag{18}$$

Next, we show $g_c,\ g_s,\ h_c$, and h_s. In the case of $c_1 > 0$ and $Y \neq 0$, we obtain

$$\begin{aligned}
g_c &= -\sqrt{\frac{X}{c_1\alpha}}(\sqrt{Q_1}\cos\Theta_1 \sin\Psi + \sqrt{Q_2}\cos\Theta_2\cos\Psi),\\
g_s &= \sqrt{\frac{X}{c_1\alpha}}(\sqrt{Q_1}\cos\Theta_1 \cos\Psi - \sqrt{Q_2}\cos\Theta_2\sin\Psi),\\
h_c &= -\sqrt{\frac{X}{c_1\alpha}}(\sqrt{Q_1}\sin\Theta_1 \sin\Psi + \sqrt{Q_2}\sin\Theta_2\cos\Psi),\\
h_s &= \sqrt{\frac{X}{c_1\alpha}}(\sqrt{Q_1}\sin\Theta_1 \cos\Psi - \sqrt{Q_2}\sin\Theta_2\sin\Psi),
\end{aligned} \tag{19}$$

where

$$\begin{aligned}
\Theta_1 &= c_1\frac{Y}{X}\int_0^T \frac{(\xi + \mathscr{X})\alpha(\tau) - Z}{Q_1(\alpha(\tau))}d\tau + \tilde{\mathscr{Y}}T + \theta_1,\\
\Theta_2 &= c_1\frac{Y}{X}\int_0^T \frac{(\xi + \tilde{\mathscr{X}})\alpha(\tau) - Z}{Q_2(\alpha(\tau))}d\tau + \mathscr{Y}T + \theta_2,
\end{aligned} \tag{20}$$

and the constants $\theta_1, \theta_2 \in [0, 2\pi)$ are uniquely determined by the initial values. These functions for $c_1 = 0$ or $Y = 0$ are obtained comparatively easily.

Finally, we have figured out the leading part of the nonlinear electromagnetic wave in the long timescale.

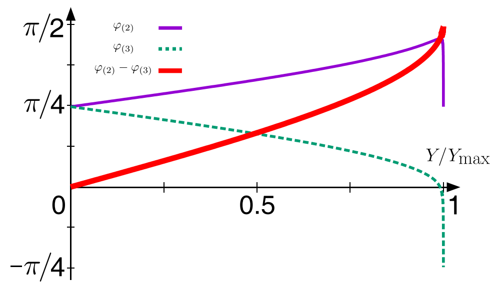

FIG. 2. The initial phases $\varphi_{(2)}$ and $\varphi_{(3)}$ as functions of Y. The conserved quantity Z introduced in Eq. (A5) is the same for every pair of $\varphi_{(2)}$ and $\varphi_{(3)}$. The red bold curve expresses the relative phase $\varphi_{(2)}-\varphi_{(3)}$, satisfying $Y \propto \sin(\varphi_{(2)}-\varphi_{(3)})$.

VI. ANGULAR MOMENTUM AFFECTS SELF-MODULATION

As we have introduced, $\alpha = (f_c^2+f_s^2)/X$ expresses the energy ratio of mode 1. Similarly, the energy ratios of modes 2 and 3 are given as $(g_c^2+g_s^2)/X$ and $(h_c^2+h_s^2)/X$, respectively. Each energy ratio can vary with time. In other words, the vacuum nonlinearity causes the energy transfer between the three modes. The behavior of the energy transfer depends on the initial values through the conserved quantities X, Y, and Z. Here we focus on Y, corresponding to the angular momentum.

Using initial values in Eq. (16), Y can be expressed as

$$Y = g_c h_s - g_s h_c = A_{(2)}A_{(3)}\sin(\varphi_{(2)}-\varphi_{(3)}). \tag{21}$$

We fix $A_{(2)}$ and $A_{(3)}$ and vary only $\varphi_{(2)}$ and $\varphi_{(3)}$ to obtain a chosen value of Y while keeping X and Z constant.

The numerical parameters are given as follows. We choose $j=3$ and $k_\rho^2/k^2 = 0.9$. Then, c_1, c_2, and $\mathscr{X}$ are $c_1/(C_{2,0}X)\approx 0.020$, $c_2/(C_{2,0}X)\approx 0.182$, and $\mathscr{X}/(C_{2,0}X)\approx 0.097$. The concrete values for a, L_z, and n are unnecessary. We further set $\xi/(C_{2,0}X)=0.03$ and $Z/(C_{2,0}X)=0.06$, corresponding to the first line in Table I at $Y=0$, where $\mathfrak{q}_{2-}\approx 0.275$ and $\mathfrak{q}_{1-}\approx 0.301$. Then, the maximum angular momentum is calculated as $Y_{\max}/X \approx 0.356$ and the corresponding intersection is $\tilde{\mathfrak{s}}\approx 0.287$. We set $\alpha(0)=\tilde{\mathfrak{s}}$ to make sure that Y can reach $Y_{\max}$. The initial energy ratios are $A_{(1)}^2/X = \tilde{\mathfrak{s}} \approx 0.287$ and $A_{(2)}^2/X = A_{(3)}^2/X = (1-\tilde{\mathfrak{s}})/2 \approx 0.356$.

Equation (A5) indicates that $\varphi_{(2)}$ and $\varphi_{(3)}$ are mutually dependent for the fixed Z. Figure 2 shows the relationship between Y and the initial phases which keep Z constant.

Figure 3 shows the time evolutions of the energy ratio of each mode for $Y/Y_{\max} = 0, 0.1, 0.6, 1$. The horizontal axes are the long timescale $C_{2,0}XT$. Since $C_{2,0}X \ll 1$, appearing oscillations are extremely slower than the one cycle of $2\pi/\omega$. As in Fig. 3(a), energy ratios of the modes 2 and 3 agree at $Y=0$. As $|Y|$ increases, the time evolutions of modes 2 and 3 have different periodicity against mode 1, shown in Figs. 3(b) and 3(c). The maximum energy ratio of modes 2 or 3 reaches up to about 0.722 in Fig. 3(b). It is about twice the initial ratio 0.356. For the maximum angular momentum $Y/Y_{\max}=1$ in Fig. 3(d), the energy ratio of mode 1 remains in the initial value as is $\alpha = \tilde{\mathfrak{s}}$. The energy ratios of modes 2 and 3 are shifted in each other's half-period. A Supplemental video [27] provides the time evolution of the energy ratio as $Y/Y_{\max}$ increases from zero to unity.

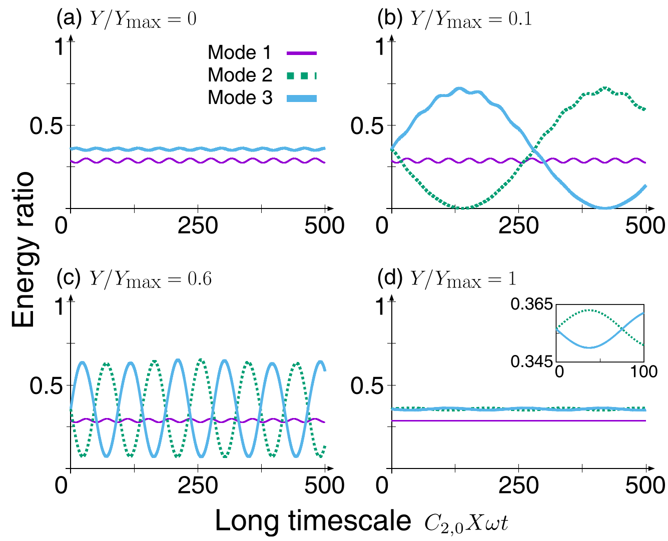

FIG. 3. Time evolutions of the energy ratios in the long timescale for (a) $Y/Y_{\max}=0$, (b) $Y/Y_{\max}=0.1$, (c) $Y/Y_{\max}=0.6$, and (d) $Y/Y_{\max}=1$.

As demonstrated in Fig. 3, the self-modulation in a long timescale is largely dependent on the value of angular momentum. It is worth emphasizing that the self-modulation depends strongly on the initial phases, not only on the amplitudes, i.e., intensity.

It will be challenging to observe these behaviors in a current experiment. In a realistic cavity, light energy is eventually lost. If we let $t_{\max}$ be the lifetime, it is typically several milliseconds for a tabletop cavity. For the visible light ($\omega \approx 10^{15}\ \mathrm{s}^{-1}$) with intensity of $10^6\ \mathrm{W/cm^2}$, we obtain $C_{2,0}X\omega t_{\max} \approx 10^{-16}$. Thus, we consider another example in the next section for a future experiment.

VII. EXPERIMENTAL PERSPECTIVE

In this example, the external magnetic field is more important than the angular momentum for a rapid emergence of the vacuum nonlinearity.

We suppose $A_{(1)}=0$, i.e., the initial state does not contain mode 1. Then, Eq. (15) is easily solved as

$$\begin{aligned}
g_c &= -A_{(2)}\sin(\epsilon T-\varphi_{(2)})\cos S_5YT \\
&\quad - A_{(3)}\sin(\epsilon T-\varphi_{(3)})\sin S_5YT, \\
g_s &= A_{(2)}\cos(\epsilon T-\varphi_{(2)})\cos S_5YT \\
&\quad + A_{(3)}\cos(\epsilon T-\varphi_{(3)})\sin S_5YT, \\
h_c &= A_{(2)}\sin(\epsilon T-\varphi_{(2)})\sin S_5YT \\
&\quad - A_{(3)}\sin(\epsilon T-\varphi_{(3)})\cos S_5YT, \\
h_s &= -A_{(2)}\cos(\epsilon T-\varphi_{(2)})\sin S_5YT \\
&\quad + A_{(3)}\cos(\epsilon T-\varphi_{(3)})\cos S_5YT,
\end{aligned} \tag{22}$$

where $\epsilon = S_4X + (k_\rho^2/k^2)C_{0,2}B_s^2$.

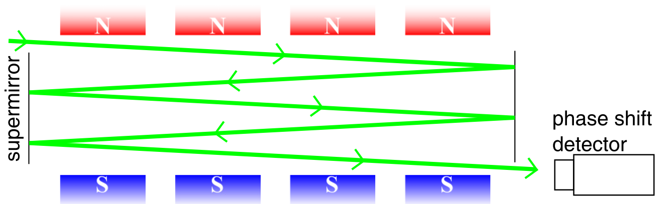

FIG. 4. A successor system for an experimental observation of vacuum nonlinearity. The incident light is depicted by a green zigzag line. It is modulated by the external magnets. The phase shift will be observed in the detector.

The electric field at $\theta = 0$ and $z = 0$ is approximated by

$$E_z(\rho, 0, 0) \approx \frac{k_\rho}{k} J_1(k_\rho \rho) \sqrt{h_c^2 + h_s^2} \sin(T + \Theta), \tag{23}$$

where the "phase" Θ is given by $\sin\Theta = h_c/\sqrt{h_c^2 + h_s^2}$ and $\cos\Theta = h_s/\sqrt{h_c^2 + h_s^2}$. The phase slowly varies with time due to the vacuum nonlinearity. The phase shift $\Delta\Theta = \Theta(t) - \Theta(0)$ can be controlled by the external magnetic field B_s. If both $|\epsilon\omega t_{\max}|$ and $|S_5 Y \omega t_{\max}|$ are much smaller than unity, we obtain

$$\Delta\Theta \approx -\left[S_5 A_{(2)}^2 \sin^2(\varphi_{(2)} - \varphi_{(3)}) + S_4 X + \frac{k_\rho^2}{k^2} C_{0,2} B_s^2\right] \omega t. \tag{24}$$

In particular, if the external magnetic field is much stronger than the light intensity I, i.e., $B_s^2 \gg (\mu_0/c)I$ (in SI units), we can evaluate the maximum phase shift by

$$|\Delta\Theta| \approx 10^{-9} B_s^2 t_{\max}, \tag{25}$$

where B_s is in SI units, and we applied $\omega = 10^{15}\ \mathrm{s}^{-1}$.

The magnitude of the static magnetic field is currently several tens of tesla [28]. $B_s \approx 10^2$ T will be achieved in the near future. How can we evaluate $t_{\max}$? Suppose the vacuum nonlinearity is detectable if 1% of incident light remains. The mirror is supposed to be a supermirror with a reflectivity of 99.9999%. Let L be the typical length between the mirrors. Then, we can evaluate $t_{\max}$ by $0.999\,999^{ct_{\max}/L} = 0.01$. If the cavity size is huge as LIGO [29], $L \approx 10^3$ m yields $t \approx 15$ s. Finally, $|\Delta\Theta| \approx 10^{-4}$ rad.

This estimation is somewhat artificial, as the original calculation is performed for a closed cavity with perfect mirrors. Moreover, it is not realistic to impose a uniform magnetic field for the whole cavity of kilometer size.

A system in Fig. 4 will be a next step. An open cavity is composed of supermirrors. The external magnetic field is imposed perpendicular to the cavity. Multiple magnets cover the whole cavity. The light is irradiated with a shallow angle. The phase shift of outgoing light is measured. The calculation of this system can be done by the extended FDTD method [21].

In a practical system, the dissipation, i.e., the energy loss by mirror reflection, will be important. It can be handled in the extended FDTD calculation by adopting realistic boundary conditions for the mirror surface. The dissipation by mirrors is often treated in a different manner. It uses the phenomenological quality factor Q through the damping term of $(\omega/Q)\partial_t$ [19,20]. The latter manner will also be included in the extended FDTD method. The difference between both treatments is also interesting. In this study, the quality factor has not been employed because it is incompatible with the assumption of a perfect conductor mirror.

VIII. FINAL REMARKS

We have analyzed a nonlinear electromagnetic wave in a cylindrical cavity, especially from the viewpoint of angular momentum. Equations (15) are derived by the secular term in Eq. (10). The differential equations describe the self-modulation in the long timescale. We have demonstrated how the angular momentum changes the self-modulation. In particular, it has been elucidated that the energy transfer depends strongly on the initial phases. We refer to the contribution of the external field B_s. A large nonlinear behavior emerges sooner as the value becomes larger, as shown in Sec. VII and prior studies [21,22].

A third-harmonic wave can increase resonantly if the cavity size a/L_z satisfies a specific condition [19]. To broaden the chance of a verification experiment on the vacuum nonlinearity, it will be useful to analyze the high harmonics and other sum and difference frequencies, as performed in a rectangular cavity [20].

For a future verification experiment, we have considered another example where the external magnetic field plays an important role in this case. It will be worth pursuing a large open-cavity system with supermirrors and an external magnetic field.

The revealed behavior of the nonlinear electromagnetic wave in the cavity and the analysis method that we performed will be of great merit for further studies of the QED vacuum.

ACKNOWLEDGMENTS

The authors thank Dr. M. Nakai, Dr. K. Mima, and Dr. K. Seto for discussion. In addition, we appreciate the help of Dr. J. Gabayno and K. E. Juadines in checking the logical consistency of the text.

APPENDIX: SOLUTION METHOD OF EQ. (15)

In this Appendix, an auxiliary function α is introduced and solved. Its typical behavior is also shown. During the process, we obtain another conserved quantity Z.

1. Reduction of functions

There are six unknown functions in Eq. (15). By introducing the following five functions:

$$\begin{aligned}
\alpha &= \frac{1}{X}(f_c^2 + f_s^2),\\
\beta_2 &= \frac{1}{X}(f_c g_c + f_s g_s), \quad \beta_3 = \frac{1}{X}(f_c h_c + f_s h_s),\\
\gamma_2 &= \frac{1}{X}(f_c g_s - f_s g_c), \quad \gamma_3 = \frac{1}{X}(f_c h_s - f_s h_c),
\end{aligned} \tag{A1}$$

reduced equations that contain only the five unknown functions are obtained:

$$\begin{aligned}
\dot{\alpha} &= c_1(\beta_2\gamma_2 + \beta_3\gamma_3),\\
\dot{\beta}_2 &= (c_2\alpha - \xi - \mathscr{X})\gamma_2 - \mathscr{Y}\beta_3,\\
\dot{\beta}_3 &= (c_2\alpha - \xi - \mathscr{X})\gamma_3 + \mathscr{Y}\beta_2,\\
\dot{\gamma}_2 &= -(\tilde{c}_2\alpha - \xi - \tilde{\mathscr{X}})\beta_2 - \tilde{\mathscr{Y}}\gamma_3,\\
\dot{\gamma}_3 &= -(\tilde{c}_2\alpha - \xi - \tilde{\mathscr{X}})\beta_3 + \tilde{\mathscr{Y}}\gamma_2,
\end{aligned}\tag{A2}$$

where

$$\begin{aligned}
c_1 &= -2S_3X,\\
c_2 &= (S_1 - 2S_2 + S_4)X,\quad \tilde{c}_2 = c_2 + c_1,\\
\mathscr{X} &= (S_4 - S_2)X,\quad \tilde{\mathscr{X}} = \mathscr{X} + \frac{1}{2}c_1,\\
\mathscr{Y} &= (S_3 - S_5)Y,\quad \tilde{\mathscr{Y}} = \mathscr{Y} + \frac{Y}{X}c_1,\\
\xi &= -\frac{k_\rho^2}{k^2}(4C_{2,0} - C_{0,2})B_s^2.
\end{aligned}\tag{A3}$$

In particular, $\alpha \in [0, 1]$ expresses the energy ratio of mode 1.

The pair of second and third lines in Eq. (A2) yields a first integral. By defining

$$\begin{aligned}
Q_1(\alpha) &= c_2\alpha^2 - 2(\xi + \mathscr{X})\alpha + Z,\\
Q_2(\alpha) &= c_1\alpha(1-\alpha) - Q_1(\alpha),
\end{aligned}\tag{A4}$$

where Z is another conserved quantity, we obtain

$$\begin{aligned}
c_1\left(\beta_2^2 + \beta_3^2\right) &= Q_1(\alpha),\\
c_1\left(\gamma_2^2 + \gamma_3^2\right) &= Q_2(\alpha).
\end{aligned}\tag{A5}$$

The magnitude of Z is of the order of $C_{2,0}X$. This parameter is purely mathematical.

2. Constraints on parameters

We clarify the magnitude relations among the parameters. As for the two integrals I_+ and I_- in Eq. (12), I_+ diverges and I_- converges to $1/\pi^2$ [30,31] as $j \to \infty$. Therefore, the following inequalities hold for $j \geqslant 3$:

$$\begin{aligned}
0 &< \tfrac{1}{2}c_2 < \mathscr{X} < c_2,\\
0 &< \tfrac{1}{2}\tilde{c}_2 < \tilde{\mathscr{X}} < \tilde{c}_2.
\end{aligned}\tag{A6}$$

The possible range of Z depends on the external magnetic flux density B_s through ξ. For $c_1 \geqslant 0$ and $j \geqslant 3$, the range is given by

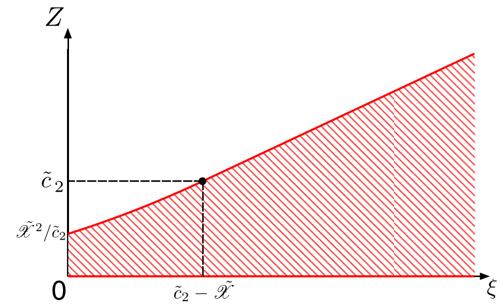

FIG. 5. The possible range of Z for each ξ shown in Eq. (A7).

$$\begin{aligned}
&0 \leqslant Z \leqslant \frac{1}{\tilde{c}_2}(\xi + \tilde{\mathscr{X}})^2 \quad (0 \leqslant \xi \leqslant \tilde{c}_2 - \tilde{\mathscr{X}}),\\
&0 \leqslant Z \leqslant 2\xi + 2\tilde{\mathscr{X}} - \tilde{c}_2 \quad (\tilde{c}_2 - \tilde{\mathscr{X}} \leqslant \xi),
\end{aligned}\tag{A7}$$

as shown in Fig. 5. The possible range for $c_1 \leqslant 0$ and $j \geqslant 3$ is obtained by replacing $\tilde{c}_2$ and $\tilde{\mathscr{X}}$ by c_2 and $\mathscr{X}$, respectively. We suppose $c_1 \geqslant 0$ in the following.

3. Equation for only α

Defining a quartic polynomial

$$P(\alpha) = Q_1(\alpha)Q_2(\alpha) - c_1^2\frac{Y^2}{X^2}\alpha^2, \tag{A8}$$

the differential equation for only α is obtained:

$$\dot{\alpha}^2 = P(\alpha). \tag{A9}$$

Obviously, α moves in the region of $P(\alpha) \geqslant 0$. Depending of the multiplicity of the roots of P, the behavior of α is classified into three categories: "oscillates," "reflects at most once and converges," and "remains in the initial value."

The solution of Eq. (A9) is given as follows [22]. In the case of oscillation, α is a periodic function. Once the minimum and maximum values are determined, α can be described by Jacobi's elliptic function sn. If α converges, $\dot{\alpha}$ changes its sign at most once. Hence, α can be obtained by integrating $\dot{\alpha} = \pm\sqrt{P}$ at most twice by choosing a correct sign.

The remaining task is to specify the roots of P which determine the behavior of α. All the roots can be calculated by the quartic formula. However, this method inevitably includes complex numbers, known as "*casus irreducibilis*" [32]. It is hard to distinguish which root is an upper or lower limit of α. Thus, we treat the cases $Y = 0$ and $Y \neq 0$ separately.

TABLE I. The minimum and maximum values of oscillating α and corresponding ranges of ξ and Z. The symbol $\wedge$ is a logical conjunction.

Range of α	Ranges of ξ and Z
$[\mathfrak{q}_{2-}, \mathfrak{q}_{1-}]$	$0 \leqslant \xi < c_2 - \mathscr{X} \wedge 0 < Z < (\xi + \mathscr{X})^2/c_2$ or $c_2 - \mathscr{X} \leqslant \xi \wedge 0 < Z < 2\xi + 2\mathscr{X} - c_2$
$[\mathfrak{q}_{1+}, \mathfrak{q}_{2+}]$	$0 \leqslant \xi < c_2 - \mathscr{X} \wedge 2\xi + 2\mathscr{X} - c_2 < Z < (\xi + \mathscr{X})^2/c_2$
$[\mathfrak{q}_{2-}, \mathfrak{q}_{2+}]$	$0 \leqslant \xi < c_2 - \mathscr{X} \wedge (\xi + \mathscr{X})^2/c_2 < Z < (\xi + \tilde{\mathscr{X}})^2/\tilde{c}_2$ or $c_2 - \mathscr{X} \leqslant \xi < \tilde{c}_2 - \tilde{\mathscr{X}} \wedge 2\xi + 2\mathscr{X} - c_2 < Z < (\xi + \tilde{\mathscr{X}})^2/\tilde{c}_2$

TABLE II. The limit values of converging α and corresponding ranges of ξ and Z. The initial value $\alpha(0)$ must differ from the limit value.

Limit value of α	Ranges of ξ and Z
$\mathfrak{q}_1$	$0 \leqslant \xi < c_2 - \mathscr{X} \wedge Z = (\xi + \mathscr{X})^2/c_2$
1	$c_2 - \mathscr{X} \leqslant \xi < \tilde{c}_2 - \tilde{\mathscr{X}} \wedge Z = 2\xi + 2\mathscr{X} - c_2$

4. Behavior of α for $Y = 0$

In this case, $P(\alpha) = Q_1(\alpha)Q_2(\alpha)$. We notate the roots of $Q_1(\alpha)$ and $Q_2(\alpha)$ as $\mathfrak{q}_{1\pm} = \{\xi + \mathscr{X} \pm [(\xi + \mathscr{X})^2 - c_2 Z]^{1/2}\}/c_2$ and $\mathfrak{q}_{2\pm} = \{\xi + \tilde{\mathscr{X}} \pm [(\xi + \tilde{\mathscr{X}})^2 - \tilde{c}_2 Z]^{1/2}\}/\tilde{c}_2$, respectively. If the roots are a double root, they are notated as $\mathfrak{q}_1$ and $\mathfrak{q}_2$, respectively.

The category of α is determined by ξ and Z. For each category, characteristic values of α and corresponding ranges of ξ and Z are summarized in Tables I, II, and III, respectively.

5. Behavior of α for $Y \neq 0$

α can move in the region of $Q_1Q_2 \geqslant (c_1Y/X)^2\alpha^2$. Thus, α can be solved by obtaining the intersections of Q_1Q_2 and $(c_1Y/X)^2\alpha^2$. Figure 6 shows an example for certain c_1, c_2, $\mathscr{X}$, ξ, and Z. The black and red curves express Q_1Q_2 and $(c_1Y/X)^2\alpha^2$, respectively. α oscillates between $[\mathfrak{p}_1(Y), \mathfrak{p}_2(Y)]$, where $\mathfrak{p}_1(Y), \mathfrak{p}_2(Y), \ldots$ are the roots of P, i.e., intersections of Q_1Q_2 and $(c_1Y/X)^2\alpha^2$ existing in $[\mathfrak{q}_{2-}, \mathfrak{q}_{2+}]$ in ascending order.

TABLE III. For stationary α, its value and corresponding ranges of ξ and Z.

Stationary value of α	Ranges of ξ and Z
0	$0 \leqslant \xi \wedge Z = 0$
$\mathfrak{q}_1$	$0 \leqslant \xi < c_2 - \mathscr{X} \wedge Z = (\xi + \mathscr{X})^2/c_2$
$\mathfrak{q}_2$	$0 \leqslant \xi < \tilde{c}_2 - \tilde{\mathscr{X}} \wedge Z = (\xi + \tilde{\mathscr{X}})^2/\tilde{c}_2$
1	$0 \leqslant \xi \wedge Z = 2\xi + 2\mathscr{X} - c_2$

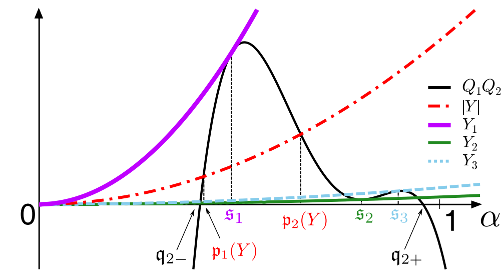

FIG. 6. An example of Q_1Q_2 and $(c_1Y/X)^2\alpha^2$ for several Y. The parameters are set to $c_1/(C_{2,0}X) = 2$, $c_2/(C_{2,0}X) = 3$, $\mathscr{X}/(C_{2,0}X) = 2$, $\xi/(C_{2,0}X) = 0.5$, and $Z/(C_{2,0}X) = 2.1$ for the visibility. In this example, $Y_{\max} = Y_1$ and $\tilde{\mathfrak{s}} = \mathfrak{s}_1$.

Before explaining the figure in detail, we refer to several Y such that Q_1Q_2 and $(c_1Y/X)^2\alpha^2$ are tangent in [0,1]. The corresponding α is a root of both P and P'. Thus, it is a solution of the following equation:

$$\frac{Q_1'}{Q_1} + \frac{Q_2'}{Q_2} = \frac{2}{\alpha}, \tag{A10}$$

which does not contain Y. We express the solutions existing in [0,1] in ascending order as $\mathfrak{s}_1, \mathfrak{s}_2, \ldots$. The maximum number is three. For each solution, there is a unique $Y_{1,2,\ldots} > 0$ such that the solution is a point of contact of Q_1Q_2 and $(c_1Y/X)^2\alpha^2$. For example, $\alpha = \mathfrak{s}_1$ is a solution of Eq. (A10) and $P(\mathfrak{s}_1) = 0$ holds. The maximum value among $Y_{1,2,\ldots}$ is the maximum value $Y_{\max}$ of Y, and the corresponding solution of Eq. (A10) is notated by $\tilde{\mathfrak{s}}$.

We demonstrate how the value of Y changes the behavior of α in Fig. 6. In this case, Q_1 has complex roots, α oscillates in $[\mathfrak{q}_{2-}, \mathfrak{q}_{2+}]$ at $Y = 0$, and $Y_{\max} = Y_1$.

The behavior of α is classified as follows. (i) If $0 < |Y| < Y_2$, α oscillates between $[\mathfrak{p}_1(Y), \mathfrak{p}_2(Y)]$. (ii) If $|Y| = Y_2$, α converges to or remains in $\mathfrak{s}_2$. (iii) If $Y_2 < |Y| < Y_3$, α oscillates between $[\mathfrak{p}_1(Y), \mathfrak{p}_2(Y)]$ or $[\mathfrak{p}_3(Y), \mathfrak{p}_4(Y)]$, depending on its initial value. (iv) If $|Y| = Y_3$, α oscillates between $[\mathfrak{p}_1(Y), \mathfrak{p}_2(Y)]$ or remains in $\mathfrak{s}_3$. (v) If $Y_3 < |Y| < Y_1$, α oscillates between $[\mathfrak{p}_1(Y), \mathfrak{p}_2(Y)]$. This case is shown by the red chained curve. (vi) If $|Y| = Y_1$, α remains in $\tilde{\mathfrak{s}} = \mathfrak{s}_1$.

[1] E. Heisenberg and Köckel, Naturwiss. **23**, 246 (1935).
[2] W. Heisenberg and H. Euler, Z. Phys. **98**, 714 (1936).
[3] M. Born, L. Infeld, and R. H. Fowler, Proc. R. Soc. London, Ser. A **144**, 425 (1934).
[4] J. Plebanski, *Lectures on Non-Linear Electrodynamics: An Extended Version of Lectures Given at the Niels Bohr Institute and NORDITA, Copenhagen, in October 1968* (NORDITA, Copenhagen, 1970).
[5] K. A. Bronnikov, Phys. Rev. D **63**, 044005 (2001).
[6] J. S. Heyl and L. Hernquist, Astrophys. J. **618**, 463 (2005).
[7] S. Shakeri, M. Haghighat, and S.-S. Xue, J. Cosmol. Astropart. Phys. 10 (2017) 014.
[8] R. P. Mignani, V. Testa, K. Wu, S. Zane, D. Gonzalez Caniulef, R. Turolla, and R. Taverna, Mon. Not. R. Astron. Soc. **465**, 492 (2017).
[9] E. Ayon-Beato and A. García, Phys. Lett. B **464**, 25 (1999).
[10] I. TURCU, F. Negoita, D. Jaroszynski, P. Mckenna, S. Balascuta, D. Ursescu, I. Dancus, M. Cernaianu, M. Tataru, P. Ghenuche, D. Stutman, A. Boianu, M. Risca, M. Toma, C. Petcu, G. Acbas, S. Yoffe, A. Noble, B. Ersfeld, and N. Zamfir, Rom. Rep. Phys. **68**, S145 (2016).
[11] G. Brodin, M. Marklund, and L. Stenflo, Phys. Rev. Lett. **87**, 171801 (2001).
[12] V. I. Denisov and I. P. Denisova, Opt. Spectrosc. **90**, 282 (2001).
[13] F. Della Valle, E. Milotti, A. Ejlli, G. Messineo, L. Piemontese, G. Zavattini, U. Gastaldi, R. Pengo, and G. Ruoso, Phys. Rev. D **90**, 092003 (2014).
[14] F. D. Valle, U. Gastaldi, G. Messineo, E. Milotti, R. Pengo, L. Piemontese, G. Ruoso, and G. Zavattini, New J. Phys. **15**, 053026 (2013).

[15] A. Cadène, P. Berceau, M. Fouché, R. Battesti, and C. Rizzo, Eur. Phys. J. D **68**, 16 (2014).
[16] X. Fan, S. Kamioka, T. Inada, T. Yamazaki, T. Namba, S. Asai, J. Omachi, K. Yoshioka, M. Kuwata-Gonokami, A. Matsuo, K. Kawaguchi, K. Kindo, and H. Nojiri, Eur. Phys. J. D **71**, 308 (2017).
[17] K. Shibata, Eur. Phys. J. D **74**, 215 (2020).
[18] K. Shibata, Eur. Phys. J. D **75**, 169 (2021).
[19] D. Eriksson, G. Brodin, M. Marklund, and L. Stenflo, Phys. Rev. A **70**, 013808 (2004).
[20] I. Kopchinskii and P. Satunin, Phys. Rev. A **105**, 013508 (2022).
[21] K. Shibata, Phys. Rev. A **104**, 063513 (2021).
[22] K. Shibata, Eur. Phys. J. D **76**, 216 (2022).
[23] J. Schwinger, Phys. Rev. **82**, 664 (1951).
[24] M. Fouché, R. Battesti, and C. Rizzo, Phys. Rev. D **93**, 093020 (2016).
[25] R. Baier, A. Rebhan, and M. Wödlinger, Phys. Rev. D **98**, 056001 (2018).
[26] K. Shibata, Phys. Scr. **97**, 025506 (2022).
[27] See Supplemental Material at http://link.aps.org/supplemental/10.1103/PhysRevA.109.063503 for a supplemental video that shows the time evolution of the energy ratio. The initial values and parameters are the same as Fig. 3, except for the value of $Y/Y_{\max}$.
[28] G. Majkic, R. Pratap, M. Paidpilli, E. Galstyan, M. Kochat, C. Goel, S. Kar, J. Jaroszynski, D. Abraimov, and V. Selvamanickam, Supercond. Sci. Technol. **33**, 07LT03 (2020).
[29] B. P. Abbott *et al.* (LIGO Scientific Collaboration and Virgo Collaboration), Phys. Rev. Lett. **116**, 061102 (2016).
[30] I. S. Gradshteyn and I. M. Ryzhik, *Table of Integrals, Series, and Products*, 7th ed. (Academic, London, 2007).
[31] H. Bateman, *Higher Transcendental Functions* (McGraw-Hill, New York, 1953), Vol. 2.
[32] J. Rotman, *Galois Theory* (Springer, New York, 1998).